6-Methoxy-3,3',3'-trimethylspiro[2H-1-benzopyran-2,1'[2]oxaindan]: Separation of Enantiomers, Circular Dichroism Measurements and Determination of the Absolute Configuration

Elena N. Voloshina, Yuekui Wang, Nikolai A. Voloshin[a], Gerhard Raabe, Hans-Joachim Gais, and Jörg Fleischhauer

Institut für Organische Chemie, Rheinisch-Westfälische Technische Hochschule Aachen, Prof.-Pirlet-Strasse, 1, D-52074 Aachen
[a] Institute of Physical and Organic Chemistry, Rostov State University, 344090 Rostov on Don, Russia

Reprint requests to Prof. J. F.; E-mail: Joerg.Fleischhauer@thc.rwth-aachen.de; Fax: +49(0)241/8092385.

Z. Naturforsch. **58a,** 443 – 450 (2003); received June 7, 2003

The enantiomers of 6-methoxy-3,3',3'-trimethylspiro[2H-1-benzopyran-2,1'[2]oxaindan] were separated with the high-pressure liquid chromatography method. Their optical properties were studied experimentally and by quantum-chemical calculations. The absolute configurations of the compounds were determined by comparison of the measured and calculated CD spectra.

Key words: Spiropyrans; Circular Dichroism; TDDFT Calculations.

1. Introduction

Spiropyrans represent a class of organic photochroms [1 – 3]. The discovery of the photochromic reaction of spiropyrans by Fischer and Hirshberg in 1952 [4], and Hirshberg's idea of using this phenomenon for a photochemically erasable memory [5] initiated active research on photochromic spiropyrans. Based on their reversible colour and other changes in physical and chemical properties, these photoresponsive materials have now found many applications: self-developing photography, displays, optical filters, lenses of variable optical density, including sun glasses, optical recording media, etc. [1, 6 – 10]. The photochromic (and also thermochromic) behavior of these compounds is due to the interconversion between the colourless closed spiropyran and the opened merocyanine-like dye (Scheme 1). Owing to the presence of the stereogenic C_{spiro} atom, the spiropyran molecules are chiral.

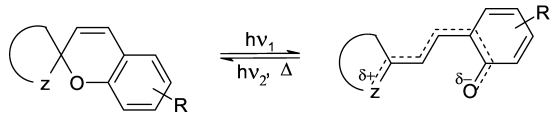

closed spirocyclic form — opened merocyanine-like structure

Scheme 1.

An enantiomerically pure, optically active spiropyran could be the object of several interesting experiments [3, 8, 11, 12], but laboratory procedures normally give a 1:1 mixture of both enantiomers. Successful attempts to separate the spiropyran enantiomers have already been undertaken by Mannschreck and coworkers [12 – 14], but the absolute configuration of the stereoisomers has not been determined and still remains unknown. In this paper, we describe the separation of the enantiomers of 6-methoxy-3,3',3'-trimethylspiro[2H-1-benzopyran-2,1'[2]oxaindan] (**1**). We then measured the UV and CD spectra of both enantiomers and tried to determine the absolute configuration by comparison of the experimental CD spectra with the calculated ones.

2. Results and Discussion

Separation of the enantiomers and their optical properties. The enantiomers of **1** (Fig.1) were separated with the high-pressure liquid chromatography (HPLC) method [12].

The experimental CD spectrum of one of the enantiomers of **1**, recorded in MeOH, is shown in Figure 2. The *Cotton* effects at wavelengths > ca. 250 nm are very broad and relatively weak while those below this value are not only much stronger but also signifi-

Table 1. Experimental ($\lambda_{max,exp}$, $\varepsilon_{max,exp}$) and calculated ($\lambda_{max,cal}$, $\varepsilon_{max,cal}$) UV spectra of spiropyran **1** in MeOH. λ_{max} in nm, ε_{max} in $l \cdot cm^{-1} \cdot mol^{-1}$.

No.	$\lambda_{max,exp}$	$\varepsilon_{max,exp}$	$\lambda_{max,cal}$	$\varepsilon_{max,cal}$
1	316	3326	351.9	3257
2	256	7756	264.3	18468
3	228	23441	216.7	29351
4	211	25239	192.7	31935

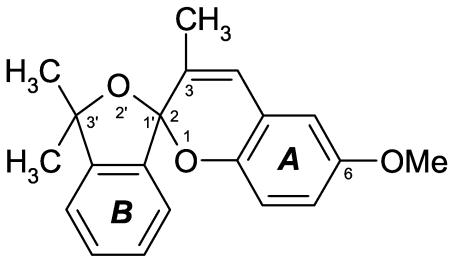

Fig. 1. 6-Methoxy-3,3',3'-trimethylspiro[2H-1-benzopyran-2,1'[2]oxaindan] **1**.

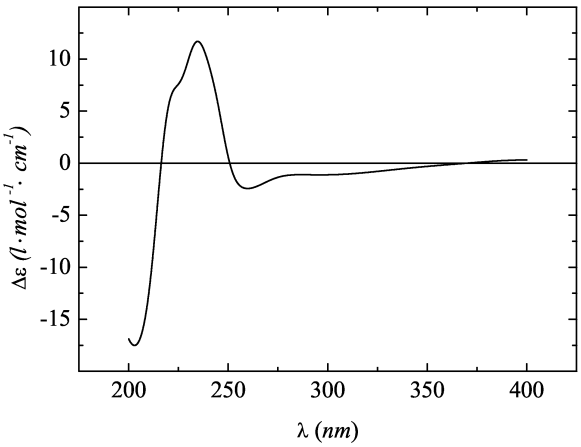

Fig. 2. Experimental CD spectrum of one of the enantiomers of **1** recorded in MeOH.

cantly sharper. The noticeable CD peaks appear at the wavelengths λ = 398.0 nm (+0.30), 296.2 nm (−1.12), 286.4 nm (−1.10), 259.7 nm (−2.43), 234.6 nm (+11.7), and 202.9 nm (−17.5). In addition, a shoulder is observed at about 225 nm (∼7.5). The numbers in parentheses are the corresponding values of $\Delta\varepsilon$ in $l \cdot mol^{-1} \cdot cm^{-1}$.

The experimental and calculated UV spectra of the studied spiropyran are given in Figure 3. Measured and calculated values of λ_{max} and ε_{max} are listed in Table 1[a)].

[a)] The first absorption band in the UV spectrum has been observed and calculated at 316 and 351.9 nm, respectively. Compared with the other bands of the spectrum, this absorption is relatively weak. According to our calculations it gets most of its intensity from the HOMO→LUMO transition at 353.1 nm (*cf.* Table 2). While a shoulder has been observed at λ = 256 nm, we calculate a relatively sharp absorption band at 264.3 nm, involving excitations within the part of the molecule containing ring A ($\Psi_{82} \rightarrow \Psi_{86}$, $\Psi_{81} \rightarrow \Psi_{83}$) as well as charge transfer from B to A ($\Psi_{78} \rightarrow \Psi_{83}$). Another transition, calculated at 258.6 nm ($\Psi_{78} \rightarrow \Psi_{83}$), will also contribute significantly to this absorption band. The strongest aborptions caused by three or more overlapping bands have been observed between 250 and 200 nm while our calculations predict intense transitions at 221.7 and 219.3 nm as well as at 189.3 and 187.4 nm, respectively.

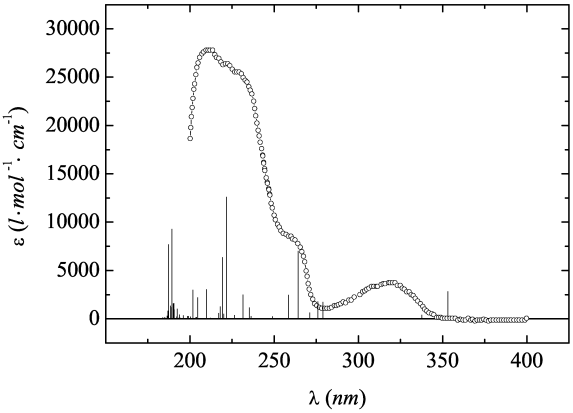

(*a*)

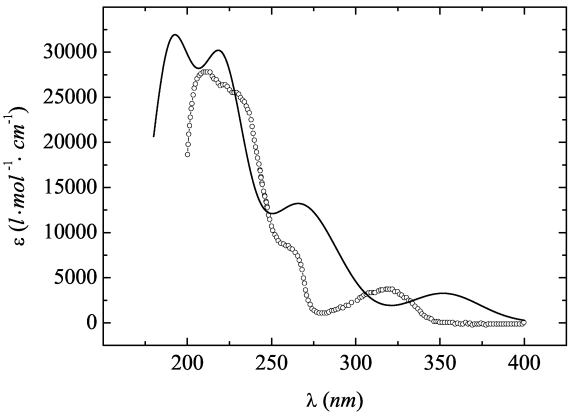

(*b*)

Fig. 3. (a) Experimental UV spectrum of the spiropyran **1** (in MeOH). The bars are the calculated ε_{max}. (b) The experimental UV spectrum of **1** (open circles) in comparison with its calculated counterpart (solid line).

Quantum-chemical calculations. The calculations have been performed for the arbitrarily chosen *R*-en-

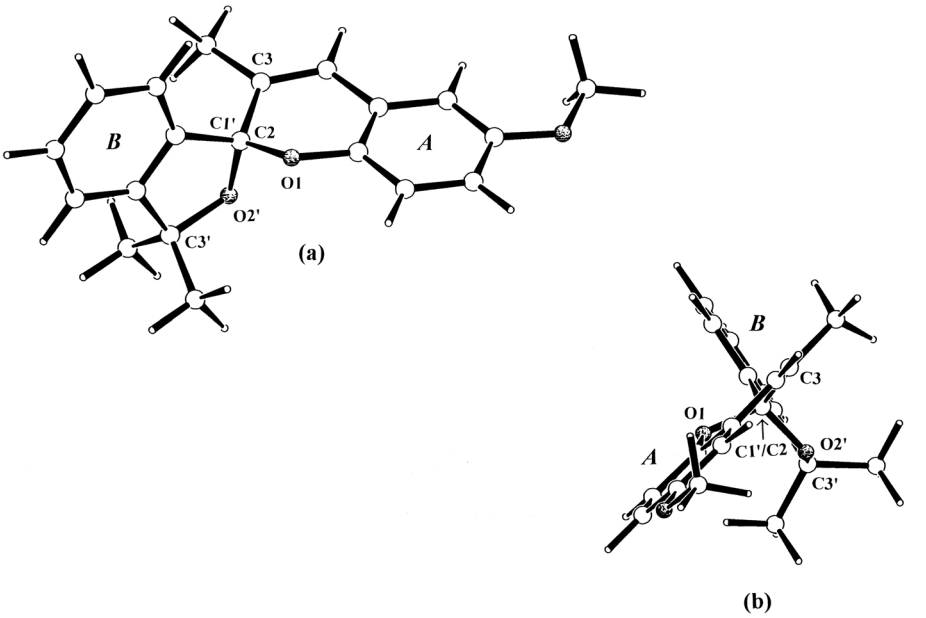

Fig. 4. Two perspective views (SCHAKAL plots [23]) of the structure of the *R*-isomer of spiropyran **1** calculated at the TZVP/B-P86 level of DFT. The structures optimized in the gas phase and in presence of the solvent are visually indistinguishable. While (a) gives a general view of the molecule (b) shows the relative orientation of the two planes containing the rings A and B, respectively.

antiomer of spiropyran **1**. The coordinates used in the CD calculation have been obtained by geometry optimization of a structure based on standard bond lengths and bond angles [15] with the density functional theory (DFT)[b]. All DFT calculations were performed using the TURBOMOLE [16] set of programs. In these calculations we used the B-P86 combination of exchange and correlation functionals [17] and a triple-ζ valence basis set, augmented by a shell of polarization functions (TZVP). The solvent effect ($\varepsilon_{CH_3OH} = 32.63$) has been taken into account by an electrostatic continuum model (COSMO, conductor-like screen model [16, 18]). Two perspective views of the optimized spatial structure of the *R*-spiropyran are shown in Figure 4.

The UV and CD spectra have been calculated with the time-dependent density functional theory (TDDFT)[19] employing the structure optimized at the DFT level (Figures 3b and 5). For the calculation of the rotational strengths the origin-independent dipole velocity approximation has been used [20].

Omitting the methyl and methoxy substituents compound **1** can approximately be described as consisting of two planes which intersect at an angle of 81.3° and share the spiro carbon atom. Each of these planes contains one of the aromatic rings A and B, respectively (Figure 1). The symmetry of the molecule is C_1 and, therefore, a strict division of the molecular orbitals into π- and σ-orbitals is not possible. However, using local symmetry we call such orbitals σ- and σ^*- or π- and π^*-MOs which are symmetric or antisymmetric with respect to one of the two planes mentioned above. The Kohn-Sham orbitals (KSOs) $\Psi_{74} - \Psi_{90}$ are shown in Figure 6. The corresponding eigenvalues of the energy cover the range between approximately -8 and 1eV, and it can be seen that each of the π- and π^*-MOs is widely localized in one of the planes containing either ring A or B.

Our TDDFT calculations in presence of MeOH predict 50 transitions in the range between 180 – 400 nm. The relevant configurations for these states are listed in Table 2 together with the calculated oscillator and rotational strengths at the absorption maxima. In addition we list the angles θ between the electric and the magnetic transition dipole moments. In cases where this angle is close to 90° the sign of the corresponding *Cotton* effect is very sensitive even to small changes of the molecular structure.

For reasons of comparison we list the corresponding data for the 50 lowest transitions calculated for the gas-phase in Table 3. All transitions are solvent-dependent as far as the excitation energies and the contributions of the leading configurations are concerned. Under the influence of the solvent the excitation wavelengths are

[b]The calculated dipole moments of the molecule obtained in the gas phase and in presence of the solvent are 2.13 and 3.43*D*, respectively.

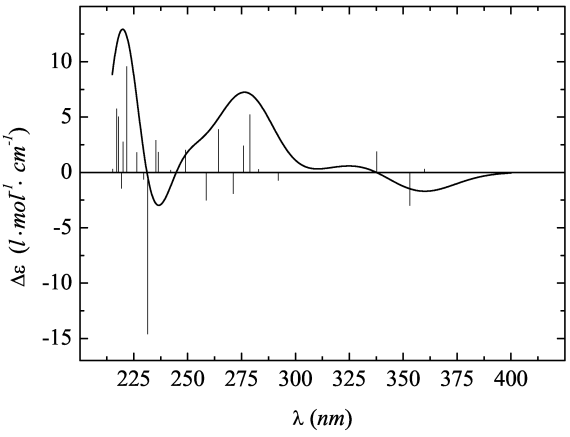

(a)

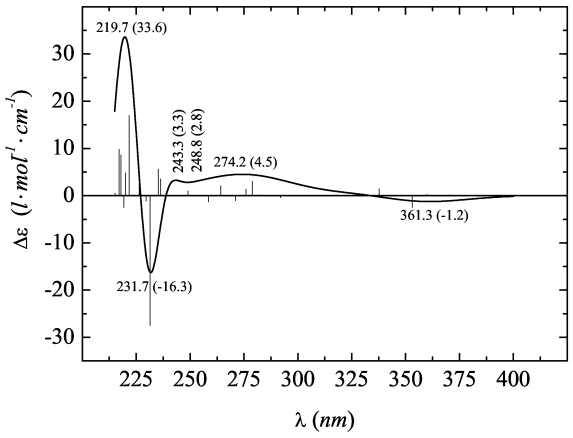

(b)

Fig. 5. CD spectrum of the spiropyran **1** (*R*-isomer) calculated at the TZVP/B-P86 level of TDDFT. The bars are the $\Delta\varepsilon_{\mathrm{max,cal}}$ of the generating Gaussian curves. Spectrum (5a) has been obtained using an empirical relationship between the half bandwidth (Γ) and the transition wavelength (see text and [22]). Spectrum (5b) has been generated using the constant values of $\Gamma = 7$ below and $\Gamma = 30$ above $\lambda = 240$ nm (numerical values of $\Delta\varepsilon_{\mathrm{max,cal}}$ in parentheses).

shifted to the blue. The strongest shift of about 24 nm has been calculated for the energetically lowest transition ($\pi \rightarrow \pi^*$), which in presence of MeOH has been predicted to occur at $\lambda = 359.8$ nm. It occurs from the HOMO (Ψ_{82}) to Ψ_{84} and has a small positive rotational strength. While Ψ_{82} has its largest coefficients at the aromatic ring A and the neighbouring olefinic double bond, Ψ_{84} is predominantly located at benzene ring B (*cf.* Figure 6). This excitation can therefore be described as an intramolecular charge transfer transition from ring A to ring B. The second excitation, calculated at λ = 353.1 nm with a much stronger negative rotational strength, occurs from the HOMO to the LUMO (Ψ_{83}) and is also a $\pi \rightarrow \pi^*$ transition. However, different from the first one, in this case both KSOs are located in the same plane and have their largest coefficients at the aromatic ring A and the adjacent olefinic double bond. The third transition calculated at 337.7 nm ($\Psi_{82} \rightarrow \Psi_{85}$), can again be described as an intramolecular charge transfer of the $\pi \rightarrow \pi^*$ type. The excitation with the most negative rotational strength (-33.90×10^{-40}erg·cm^3) above 200 nm has been calculated at 231.4 nm. It is located in the ring A and is the energetically lowest transition which involves an excitation from a σ- to a π^*-MO ($\Psi_{76} \rightarrow \Psi_{83}$). In the same region the strongest positive rotational strength (21.76×10^{-40}erg·cm^3) has been calculated for a transition at 221.7 nm. It contains almost equal contributions of a transition from ring A to B ($\Psi_{77} \rightarrow \Psi_{85}$) and another one located in A ($\Psi_{82} \rightarrow \Psi_{87}$).

The calculated CD curves (Figure 5) have been obtained as a sum of Gaussians, each of which has been centered at the wavelength of the corresponding transition and multiplied with its rotational strength [21]. Two different approaches have been used to obtain the half bandwidths (Γ) of the Gaussians. First we used the empirical formula $\Gamma = \kappa \cdot \lambda_{\mathrm{cal}}^{1.5}$, where λ_{cal} is the calculated transition wavelength and the parameter κ has been assumed to be 0.00375[c)] [22]. The resulting CD spectrum is shown in Figure 5a. According to the shape of the *Cotton* effects the experimental CD curve in Figure 2 might roughly be divided into two parts: above ~250 nm the *Cotton* effects are consistently very broad while those at wavelengths below this value are much sharper. In a second approach we therefore used two different bandwidths to model the short and the long wavelengths part of the CD curve. Thus, the Gaussians have been generated using values of $\Gamma = 7$ for $\lambda < 240$ nm and $\Gamma = 30$ for $\lambda \geq 240$ *nm* at $\Delta\varepsilon_{\mathrm{max,cal}}/e$. In both cases the empirical relationship $\Delta\varepsilon_{\mathrm{max,cal}} = 2.28 \cdot \lambda_{\mathrm{max,cal}} \cdot \Gamma^{-1} \cdot R$ (R is the rotational strength) has been used to calculate $\Delta\varepsilon_{\mathrm{max,cal}}$.

[c)] This formula yields values of Γ from 12.2 to 30.0 between 220 and 400 nm.

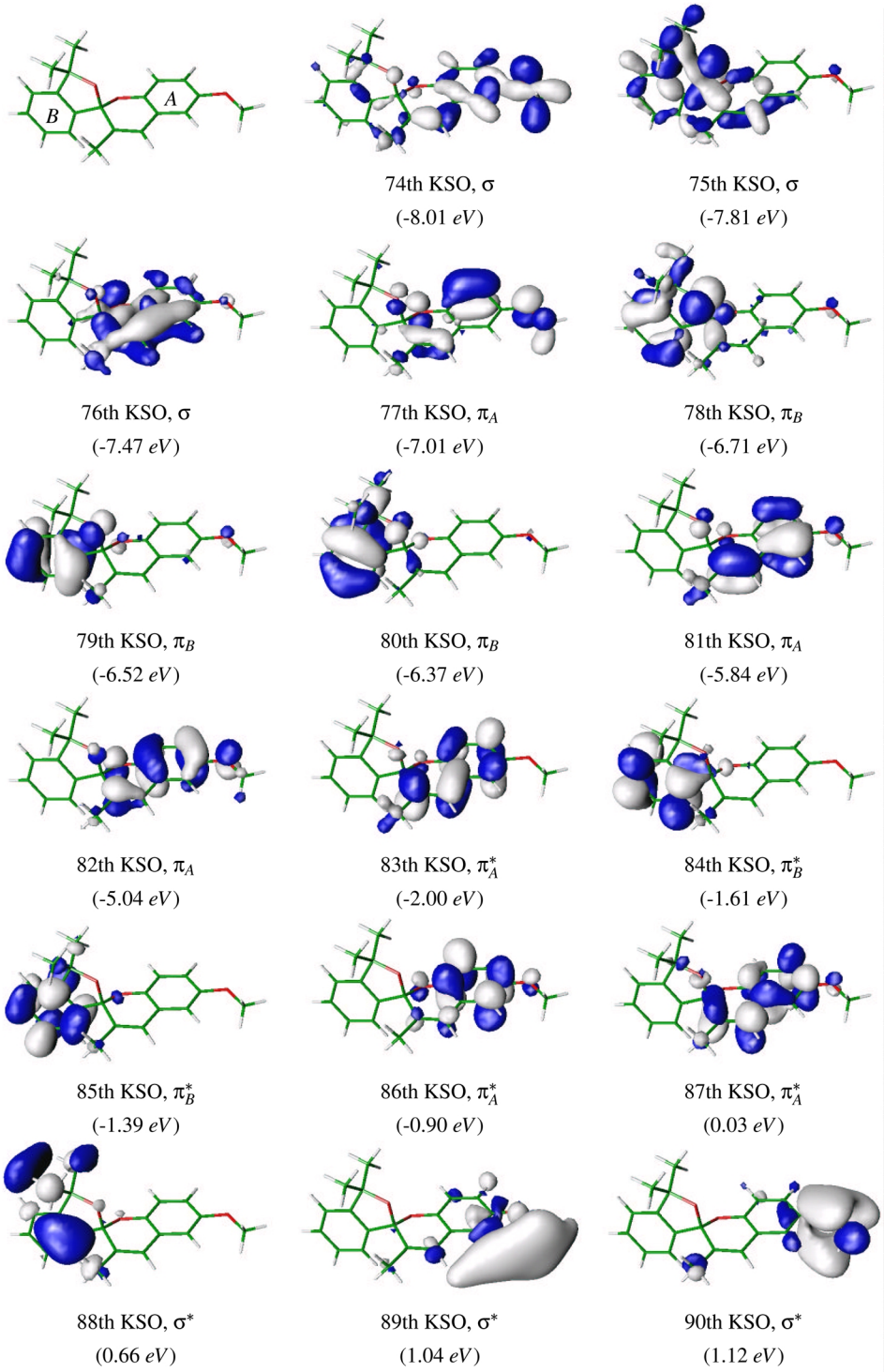

Fig. 6. Kohn-Sham orbitals Ψ_{74} to Ψ_{90} of the spiropyran **1**.

Table 2. The electronic configurations, oscillator and rotational strengths for the exited states of spiropyran **1** calculated in presence of MeOH. θ is the angle between the electric and the magnetic dipole moment.

Wavelength (nm)	Transition	Contribution (%)	θ (degree)	Oscillator Strength	Rotational Strength ($\times 10^{-40}$ erg·cm^3)
359.8	82→ 84	97.7	82.8	0.0029	0.89
353.1	82→ 83	83.6	92.9	0.0517	−8.55
337.7	82→ 85	94.9	68.5	0.0077	5.25
292.0	81→ 84	99.5	135.6	0.0011	−1.86
282.9	80→ 83	99.0	67.4	0.0008	0.69
278.9	81→ 85	70.0	81.8	0.0507	13.32
275.9	79→ 83	35.6	87.0	0.0539	6.07
	81→ 85	26.9			
	81→ 83	22.7			
271.1	79→ 83	53.2	92.6	0.0197	−4.82
	82→ 86	21.0			
264.3	82→ 86	37.5	85.6	0.2299	9.61
	81→ 83	20.3			
	78→ 83	16.3			
258.6	78→ 83	74.9	92.3	0.0847	−6.18
249.1	80→ 84	63.5	72.1	0.0089	4.87
	79→ 85	15.3			
242.1	78→ 84	40.2	73.0	0.0004	0.50
	79→ 85	24.9			
	79→ 84	22.5			
236.4	77→ 83	63.8	82.2	0.0058	4.29
	78→ 85	8.4			
235.2	78→ 85	50.8	75.2	0.0256	6.77
	80→ 85	17.2			
231.4	81→ 86	62.8	102.3	0.0569	−33.90
	76→ 83	14.7			
229.6	77→ 84	93.1	162.0	0.0003	−1.46
226.4	80→ 86	89.9	64.8	0.0084	4.13
221.7	77→ 85	37.7	80.1	0.3140	21.76
	82→ 87	35.3			
220.0	79→ 86	61.8	61.9	0.0124	6.26
	76→ 83	15.4			
219.3	77→ 85	42.3	92.0	0.1616	−3.23
	82→ 87	23.4			
217.9	76→ 83	37.1	77.0	0.0320	11.29
	75→ 83	14.9			
	79→ 86	12.0			
217.1	82→ 88	90.0	43.4	0.0153	12.90
215.3	79→ 84	22.3	44.2	0.0012	0.66
	76→ 84	20.5			
	80→ 85	16.2			
212.3	78→ 86	77.1	65.8	0.0024	2.71
209.9	76→ 84	65.2	50.3	0.0163	13.80
	80→ 85	10.8			
209.8	75→ 83	51.0	107.6	0.0842	−32.99
	78→ 86	10.9			
204.6	74→ 83	73.5	123.9	0.0646	−13.00
203.8	76→ 85	84.6	69.7	0.0042	3.08
203.5	82→ 89	91.5	85.0	0.0044	1.39
201.7	73→ 83	70.6	91.1	0.0893	−0.57
200.2	82→ 90	89.7	53.1	0.0065	6.00
199.1	75→ 84	97.1	139.1	0.0076	−4.65
198.6	82→ 91	97.3	131.0	0.0082	−11.53
196.0	82→ 92	96.3	48.0	0.0108	6.93
194.2	72→ 83	72.8	135.3	0.0027	−2.54
193.7	74→ 84	45.3	80.4	0.0132	7.81
	80→ 87	41.4			
193.4	80→ 87	49.3	106.0	0.0027	−1.36
	74→ 84	48.4			
192.5	75→ 85	69.5	102.1	0.0336	−23.4
192.2	82→ 93	85.9	85.6	0.0069	1.52
190.6	81→ 88	34.4	56.1	0.0316	47.31
	77→ 86	15.3			
	79→ 87	10.5			
	76→ 86	10.3			
190.5	81→ 88	59.6	87.2	0.0540	7.14
190.1	73→ 84	61.1	104.3	0.0536	−32.84
189.3	73→ 84	19.8	104.4	0.3172	−150.23
	79→ 84	16.5			
	80→ 85	14.6			
	77→ 86	10.5			
189.1	71→ 83	44.9	93.2	0.0403	−4.63
	79→ 87	37.1			
188.5	79→ 87	31.3	66.9	0.0461	33.75
	71→ 83	28.8			
187.4	79→ 85	23.2	88.8	0.2695	7.15
	80→ 84	15.7			
	71→ 83	8.9			
186.8	74→ 85	83.7	87.7	0.0282	3.53
186.4	82→ 94	93.4	87.9	0.0101	1.54
185.1	70→ 83	80.3	104.8	0.0053	−5.81
183.8	78→ 87	61.6	68.7	0.0043	7.03

The resulting CD spectrum is shown in Figure 5b. The signs of the *Cotton* effects in Figs. 5a and 5b and, therefore, the characteristics of both calculated spectra agree.

A comparison of the experimental and the calculated CD spectra in Figs. 2 and 5a,b shows that the signs of the *Cotton* effects in the theoretical spectrum calculated for *R*-**1** are essentially opposite to the experimental ones. Thus, we conclude that the enantiomer investigated experimentally should have the *S*-configuration[d].

[d] Note that use of two different values of Γ results in a much better agreement between the shapes of the calculated and measured CD curves than use of the empirical function $\Gamma = \kappa \cdot \lambda_{cal}^{1.5}$.

3. Experimental Part

High-pressure liquid chromatography was performed on a chiracel-OD coulumn with *n*-hexane/ ethanol (*v:v* = 89:1, column 200 × 20 mm, flow rate 6 ml·min^{-1}, pressure 11 bar) as eluent. The injected quantities of the racemates were in the range of 10 mg in 1 ml of eluent. For photomeric detection the absorption of the compound at 365 nm was used.

The CD spectra were measured using a Circular Dichroism spectrometer (AVIV Model 62DS) at room temperature in methanol.

Acknowledgements

The authors gratefully acknowledge financial support by the Deutsche Forschungsgemeinschaft and the Fonds der Chemischen Industrie. E. N. V. is thankful

Table 3. The electronic configurations, calculated oscillator and rotational strengths for the exited states of spiropyran **1** in vacuum.

Wavelength (nm)	Transition	Contribution (%)	θ (degree)	Oscillator Strength	Rotational Strength ($\times 10^{-40}$ erg·cm^3)
384.2	82→ 84	99.9	93.2	0.0022	−0.18
364.5	83→ 85	58.6		0.0166	−10.04
	82→ 83		100.5		
	82→ 83	38.6			
351.9	82→ 83	51.2	85.9	0.0450	7.99
	82→ 85	40.9			
304.4	81→ 84	99.7	115.3	0.0011	−1.21
289.8	81→ 85	93.0	76.8	0.0146	4.52
276.2	81→ 83	37.1	85.7	0.0978	15.36
	80→ 83	29.1			
	82→ 86	19.5			
273.1	80→ 83	64.6	93.5	0.0131	−4.51
	79→ 83	12.3			
266.0	79→ 83	49.8	70.4	0.0591	11.98
	82→ 86	31.4			
262.5	79→ 83	28.2	92.7	0.2067	−11.42
	81→ 83	24.4			
	82→ 86	14.3			
	78→ 83	13.7			
257.4	78→ 83	56.5	100.9	0.0340	−10.32
	80→ 84	24.1			
254.9	80→ 84	46.1	58.4	0.0086	9.08
	78→ 83	27.2			
247.2	80→ 85	40.5	60.8	0.0057	6.82
	79→ 85	30.5			
241.4	78→ 85	42.7	67.4	0.0153	6.96
	79→ 84	24.6			
238.1	77→ 84	83.4	59.9	0.0007	1.33
237.1	77→ 83	67.5	110.6	0.0066	−9.20
234.8	82→ 88	94.3	145.0	0.0006	−2.56
229.8	81→ 86	58.0	93.5	0.0484	−7.19
	76→ 83	14.1			
227.9	77→ 85	77.6	90.6	0.0649	−0.29
224.3	82→ 89	99.6	84.1	0.0068	2.14
221.9	82→ 87	59.2	85.3	0.4579	24.54
219.6	80→ 86	52.4	150.6	0.0048	−2.43
	76→ 84	15.9			
218.3	76→ 84	38.6	55.6	0.0031	5.33
	80→ 86	23.6			
217.3	76→ 83	39.9	96.1	0.0284	−6.64
	75→ 83	12.7			
	76→ 84	12.0			
215.0	82→ 90	97.8	38.9	0.0049	8.57
213.2	79→ 86	75.4	21.5	0.0029	11.03
213.1	76→ 84	24.2	72.3	0.0044	3.51
	82→ 91	17.4			
	79→ 85	14.1			
	78→ 84	9.8			
212.3	82→ 91	72.0	82.7	0.0071	0.55
209.3	76→ 85	58.1	106.3	0.0107	−4.53
	78→ 86	31.7			
208.4	78→ 86	45.0	86.6	0.0529	2.05
	75→ 83	22.6			
	76→ 85	14.6			
206.8	82→ 92	30.8	94.3	0.0496	−2.96
	75→ 83	21.1			
	78→ 86	13.6			
	76→ 85	10.6			
206.7	82→ 92	67.9	104.0	0.0331	−11.7
203.5	75→ 84	95.9	160.7	0.0042	−5.11
202.8	74→ 83	74.3	108.8	0.0533	−7.36
202.4	81→ 88	91.0	124.3	0.0114	−4.25
200.1	82→ 93	90.9	120.7	0.0054	−3.31
199.4	73→ 83	69.1	89.9	0.0849	0.01
196.9	74→ 84	94.9	76.2	0.0032	2.22
196.5	75→ 85	88.2	128.6	0.0128	−23.6
194.6	81→ 89	99.5	96.9	0.0037	−1.08
193.0	82→ 94	97.3	117.7	0.0001	−0.80
192.7	73→ 84	86.8	80.9	0.0184	9.82
191.1	74→ 85	25.3	81.3	0.1171	45.29
	72→ 83	16.8			
	77→ 86	8.8			
	78→ 84	7.1			
191.0	72→ 83	42.8	110.7	0.0615	−59.97
	82→ 95	19.4			
	77→ 86	6.7			
190.5	82→ 95	75.4	80.1	0.0615	−59.97
190.1	82→ 96	93.6	130.9	0.0123	7.88
190.0	80→ 87	53.3	43.8	0.0047	−6.88
	74→ 85	26.7			
189.1	74→ 85	29.0	93.5	0.0072	14.87
	80→ 87	14.4			
	73→ 85	9.4			
	79→ 84	8.5			
	80→ 85	7.4			
188.5	77→ 86	25.3	96.8	0.2308	−29.21
	80→ 87	16.8			
	76→ 86	13.3			
	72→ 83	12.6			
188.0	78→ 85	16.7	91.5	0.2123	−8.75
	79→ 85	10.8			
	79→ 87	9.8			
	81→ 90	9.0			
	80→ 84	8.9			
	78→ 84	5.9			
187.6	81→ 90	86.2	105.8	0.0152	−16.12

for a fellowship granted by the Graduierten Kolleg "Methoden in der Asymmetrischen Synthese". We further thank Mrs. C. Vermeeren for her technical assistance.

[1] J. C. Crano, R. Guglielmetty (eds.), Organic Photochromic and Thermochromic Compounds, Plenum Publishers, New York 1999, Vol. 1 and 2.
[2] H. Dürr, H. Bouas-Laurent (eds.), Photochromism. Molecules and Systems. Elsevier, Amsterdam 1990.
[3] R. C. Bertelson, in Techniques of Chemistry. Vol. 3, Photochromism. G. H. Brown (ed.), Photochromic Processes Involving Heterolytic Cleavage. Wiley-Interscience, New York 1971.
[4] E. Fischer and Y. Hirshberg, J. Chem. Soc. **1952**, 4522.
[5] Y. Hirshberg, J. Amer. Chem. Soc. **78**, 2304 (1956).
[6] G. Bercovic, V. Krongauz, and V. Weiss, Chem. Rev. **100**, 1741 (2000).
[7] S. Kawata and Y. Kawata, Chem. Rev. **100**, 1777 (2000).
[8] B. L. Feringa, R. A. van Delden, N. Koumura, and E. D. Geertsema, Chem. Rev. **100**, 1789 (2000).

[9] J. A. Delaire and K. Nakatani, Chem. Rev. **100**, 1817 (2000).
[10] N. Tamai and H. Miyasaka, Chem. Rev. **100**, 1875 (2000).
[11] H. Rau, Chem. Rev. **83**, 535 (1983).
[12] B. Stephan, A. Mannschreck, N. A. Voloshin, N. V. Volbushko, and V. I. Minkin, Tetrahedron Lett. **31**, 6335 (1990).
[13] R. Kiesswetter, N. Pustet, F. Brandl, and A. Mannschreck, Tetrahedron: Asym. **10**, 4677 (1999).
[14] L. Loncar-Tomaskovic, K. Lorenz, A. Hergold-Brundic, D. Mrvos-Sermec, A. Nagl, M. Mintas, and A. Mannschreck, Chirality **11**, 363 (1999).
[15] J. A. Pople, and D. L. Beveridge, Approximate Molecular Orbital Theory, McGraw-Hill Book Company, New York 1970, p. 11.
[16] R. Ahlrichs, In: Encyclopedia of Computational Chemistry. P. v. R. Schleyer, Ed. TURBOMOLE, Wiley, Chichester 1998, Vol. 5, pp. 3123 – 3129.
[17] A. D. Becke, Phys. Rev. A. **5**, 3098 (1988); J. P. Perdew, Phys. Rev. B. **33**, 8822 (1986).
[18] A. Klamt, and G. Schüürmann, J. Chem. Soc., Perkin Trans. **2**, 799 (1993).
[19] F. Furche, R. Ahlrichs, C. Wachsmann, E. Weber, A. Sobanski, F. Vögtle, and S. Grimme, J. Amer. Chem. Soc. **122**, 1717 (2000).
[20] A. Moscowitz, in O. Sinanoglu (ed.), Modern Quantum Chemistry, John Wiley & Sons, Inc., New York 1965, Vol. 3, p. 21.
[21] J. A. Schellman, Chem. Rev. **75**, 323 (1975).
[22] G. Kurapkat, P. Krüger, A. Wollmer, J. Fleischhauer, B. Kramer, E. Zobel, A. Koslowski, and R. W. Woody, Biopolymers **41**, 267 (1997).
[23] E. Keller, Chem. Unserer Z. **20**, 178 (1986).